Dynamic changes in the niche and transcription trigger early murine and human pluripotent stem cell-derived liver organogenesis

Ogechi Ogoke** [1], Daniel Guiggey** [1], Sarah Thompson [1], Alexander Chiang [1], Tram Hoang Anh Nguyen [1] Daniel Berke[1], Cortney Ott [1], Allison Kalinousky [1], Claire Shamul [1], Peter Chen[3], Shatoni Ross [1], Zhaowei Chen [3], Pooja Srivastava [3], Supriya Mahajan[1,2] ,Ruogang Zhao [3], Rudiyanto Gunawan [1,4], Natesh Parashurama[1,2,3,4]

[1] Department of Chemical and Biological Engineering, University at Buffalo (State University of New York), Furnas Hall, Buffalo, NY 14260

[2] Clinical and Translation Research Center (CTRC), University at Buffalo (State University of New York), 875 Ellicott St., Buffalo, NY 14203

[3] Department of Biomedical Engineering, University at Buffalo (State University of New York), Furnas Hall, Buffalo, NY 14260

[4] Center for Cell, Gene and Tissue Engineering, University at Buffalo, State University of New York, Furnas Hall Buffalo NY 14260

* Correspondence Author: Natesh Parashurama, 906 Furnas Hall, Buffalo, NY 14260; Tel: 716-645-1201; Fax: 716-645-3822; e-mail: nateshp@buffalo.edu

** Contributed equally to this work

Running Title**: Dynamic changes in niche triggers LO**

Keywords: organogenesis, organoid, hepatic differentiation, liver development, extra-cellular matrix, CCM, hepatic nuclear network, epithelial to hepatic transition, human pluripotent stem cells, liver diverticulum, liver bud, hepatoblast

ABBREVIATIONS

AFP alpha-fetoprotein
ALB albumin
BMP4 Bone Morphogenetic Protein
BSA Bovine serum albumin
CCM Collective cell migration
CHIR Wnt pathway agonist
DMEM Dulbecco's Modified Eagle's Medium
EDTA Ethylenediaminetetraacetic acid
EGF Epidermal growth factor
EGM-2 Endothelial growth medium 2
EHT epithelial to hepatic transition
FBS fetal bovine serum
FGF2 Fibroblast growth factor-2
iPSC Induced pluripotent stem cells
HEP Hepatocyte
H + M hepatic and mesenchymal
hESC human embryonic stem cells
hPSC human pluripotent stem cells
HBs hepatoblasts
HSCs hematopoietic stem cells
HE hepatic endoderm
HFF human foreskin fibroblasts
HGF hepatocyte growth factors
HPSC Human pluripotent stem cells
IMDM Iscove's modified Dulbecco's medium
LD liver diverticulum
MES Mesoderm
MG Matrigel (growth-factor free)
PBST Phosphate buffered saline tween 20
RT-PCR Real-time polymerase chain reaction
R3 IGF-1 R3-Insulin growth factor-1
SFD Serum free-differentiation
STM Septum transversum mesenchyme
TFs Transcription factors
VEGF Vascular endothelial growth factor

AUTHOR CONTRIBUTIONS:

OO, DG, ST, AC, TN, DB, CO, AK, CS, PC, SR, ZC, PJ, SM, RZ, RG, NP: Supervising the work, Responsible for all data, figures, and text, Ensuring the authorship is granted appropriately, Ensuring that the authors approve the content and submission of the paper, Ensuring that all authors approve the content and submission of the paper, as well as edits made through the revision and production processes, Ensuring adherence to all editorial and submission policies, Identifying and declaring competing interests on behalf of all authors , Identifying and disclosing related work by any co-authors under consideration elsewhere, Archiving unprocessed data and ensuring that figures accurately present the original data.

NP: Arbitrating decisions and disputes and ensuring communication with the journal (before and after publication), sharing of any relevant information or updates to co-authors, and accountability for fulfillment of requests for reagents and resources.

ABSTRACT

Organoids bearing human stem cell-derived progenitors enable basic and applied investigation of organogenesis in a wide range of epithelial tissues. During liver organogenesis (LO), E9.5 collectively migrating hepatoblasts (MHs) arise from the E9.0 liver diverticulum (LD) and directly penetrate the surrounding mesoderm (MES) tissue, forming cell strands that link migration, differentiation, and growth. Currently, human pluripotent stem cell (hPSC) organoid protocols model the E10.5 liver bud and forward differentiation, but not the LD or the LD-derived MHs, in spite of their significance. In fact, the transcriptome underlying MHs, the niche that drives their migration, and methods to induce them from hPSC remain key questions.

We performed bioinformatics analysis of single cell RNA-seq data, *in vivo* transplantation, and *in vitro* hPSC differentiation with organoid formation, microscopy, gene and protein expression, small molecule inhibitor screening of growth, and organoid culture in bioengineered devices to assess tissue tension.

Our in depth bioinformatic analysis of early murine LO demonstrates pathway up-regulation of an unexpected wide array of soluble signaling factors, as well as cell cycle, chromatin modification, and metabolic reprogramming, in addition to a widespread cell stress-response. These findings led us hypothesize that the LD and MES tissue form a tissue complex (LD-MESC) that drives MH induction. Using this LD-MESC concept, we designed an *in vivo* transplant system, as well as a three-step *in vitro* protocol for inducing hPSC-derived MHs, both of which recapitulate liver growth, morphogenesis, differentiation. We show that Hippo signaling pathway, in agreement with murine MH data, mediates migration and growth of hPSC-MH *in vitro*. These data substantiate the LD-MESC model developed here, and directly address key challenges facing liver regenerative medicine.

Our bioinformatics, *in vitro*, and *in vivo* data all support the concept that the LD-MESC initiates LO. This concept can be used to change protocols to emphasize linking of migration, growth, with differentiation. Modeling epithelial collective migration for LO bolsters not only organogenesis studies of alternate endodermal organs, but also *in vivo* transplantation efforts, and facilitates employing migrating organoids to therapeutically target human tumor migration/metastasis.

INTRODUCTION

Chronic liver disease is escalating globally and currently affects more than 800 million people worldwide [1]. The current accepted treatment is orthotopic liver transplantation, which bears numerous limitations, and liver regenerative medicine offers a wide array of promising several alternate solutions [2], of which liver organogenesis (LO) has great potential [3]. The aim of LO is to precisely recreate liver-like, functional tissues from adult stem cells or human pluripotent stem cells (hPSC), which would supersede many limitations of existing solutions. These functional tissues can then be used to isolate patient-specific hepatocytes (HEPs), or be used *en bloc*, for various *in vitro* applications as well as therapeutic transplantation. How to fully unravel the potential of LO remains a critical question in the field.

LO establishes liver mass, microarchitecture, and numerous liver-specific functions, and is actively being investigated. Fortunately, seminal genetic investigations of mouse LO (E8.5-18.5), reviewed elsewhere [4] provide a sound scientific basis for recreating LO. Based on these principles, current methods for modeling LO with hPSC include: 1) Directed differentiation protocols [5], 2) Organoids with exogenously added mesoderm-derived tissues (MES) [6], 3) Organoids with endogenous MES [7], 4) Assembloids of interacting organoids [8] and 5) Synthetic biology-based organoids [9]. Early LO (eLO) is a stage during which early growth, differentiation, and migration are coordinated. In eLO, the E9.0 liver diverticulum (LD), an out pocketing of tissue with only ~1500 cells, amazingly, expands by ~10^2-fold by E10 and by 10^3-fold by E11.5 [10]. The LD transitions to the E10.5 liver bud (LB) bearing the microarchitecture for forming primitive sinusoids [11]. Next, the LD initiates outward (ventral) three-dimensional (3D) collective cell migration (CCM) (E9.5) [12]. Next, hepatoblasts (HBs) that migrate (MHs) self-organize into hepatic cords, branching into adherent migrating cell stands within surrounding MES tissue [13]. This extensive morphogenesis is accompanied by highly coordinated, critical transitions in gene expression to form HBs [14]. Here, developmental gene regulatory networks (GRN) composed of master transcription factors (TFs), including FOXA2, HNF4A, PROX1, and TBX3, help initiate and maintain hepatic fate [15], boosting albumin (ALB) gene transcription [16] and triggering CCM. In summary, eLO occurs starts with the LD followed by highly impactful events. Thus far, *in vitro* hPSC studies have not focused on modeling of eLO or the LD.

Here we establish the significance of the eLO using bioinformatic analysis, *in vivo*, and *in vitro* studies. We hypothesized that the LD and surrounding MES form a tissue complex (LD-MESC) that initiates and coordinates eLO. Our bioinformatics analysis employed data from recent scRNA-seq studies that have provided several valuable insights into early LO [17-18] and support the concept of the LD-MESC. Based on our bioinformatics analysis and on *in vivo* transplantation data, here we develop a novel hPSC protocol that mimics the MH population. We provide extensive *in vitro* imaging and characterization of

the MH population, as well as mechanistic analysis which demonstrates pathways that control hLD growth and CCM.

RESULTS

Transcriptome analysis highlights coordinated up-regulation of signaling, CCM, and metabolic pathways in E9.5 migrating hepatoblasts

To elucidate the factors that drive the E9.0 LD-MESC to trigger eLO (**Fig. 1A-C**), we performed extensive bioinformatic analysis of E9.5 MHs [17]. We first analyzed the increase in ALB transcription which showed an exponential increase (**Fig. 1B**). Next, we aimed to elucidate the key regulated pathways. We assumed definitive endoderm (DE, E7.5) gives rise to gut tube (GT, E8.5), then to MH (E9.5), which then gives rise to either HB (E10.5), or hepato-mesenchyme (HM) (E10.5) (**Fig. 1C**). Our initial quality control (**Sup. Fig. 1A-D**) demonstrated clear differences between the GT, MH, and HB conditions. However, we performed re-clustering (**Sup. Fig. 1E-F**), **See Methods-Re-clustering**). To understand key regulated pathways in the MH population, we analyzed up- and down-regulated genes in GT, MH, and HB cells (initially the HM was removed), and we employed three software analysis-based approaches (REACTOME, DAVID, and ENRICHR) which we validated (**See Methods-Pathway validation, Sup File. Fig. 1**). With the set of differentially expressed genes (DEG), we first performed REACTOME analysis with pie charts for the GT, MH, and HB clusters (log2fc > 0.5, FDR < 0.05) (**Figs. 1G-J, Sup. Fig. N-O, Sup. Tables 1- 2)**. Each cell cluster was compared to the other two. Pie chart analysis for the GT population showed pathways for 898 DEG (**Sup. Fig. 1N-O, Sup. Table 2**). The MH pie chart depicting upregulated gene groups (2102 DEG), demonstrated that Signal Transduction, Transcription, Immune system, Cell Cycle, and Chromatin Organization gene groups were highest (**Fig. 1G, Sup. Table 2**). For the downregulated MH gene groups (2916 DEG), we observed that Metabolism, Metabolism of proteins, Cellular Response to Stimulus, Metabolism of RNA, were highest (**Fig. 1H, Sup. Table 2**). The HB upregulated pie chart (602 DEG), demonstrated Metabolism, and Metabolism of Proteins were higher in the HB compared to the GT and MH lineages (**Fig. 1I, Sup. Table 2**). For the downregulated HB gene groups (2550 DEG), we observed that Signal Transduction, Disease, Developmental Biology, Transcription, Cell Cycle, and Chromatin Organization, were highest (**Fig. 1J, Sup. Table 2**). The data establishes that signal transduction, transcription, cell cycle, and chromatin organization are critical within the E9.5 MH population, and are downregulated in the E10.5 HB population. This suggests the existence of a transient niche and a dynamic up-regulated and down-regulated MH-specific transcriptome, suggesting a robust switch in differentiation and phenotype.

Next, we hypothesized that up-regulation of signaling pathways is associated with changes in transcription, chromatin organization, growth (cell cycle), metabolic changes, and CCM in the MH population. Using DAVID biological process, we identified several signaling pathways significantly upregulated in MH, including MAPK, Rap 1, Hippo, Pluripotency, Insulin, FoxO, ErbB, TGF-ß, mTOR, Wnt, and NF-κB (**Fig. 1K, Sup. Table 3**). We also identified cancer/disease pathways which were up-regulated (prostate, lung, renal cell, pancreatic, colorectal, endometrial, thyroid) (**Fig. 1K, Sup. Table 3**). Interestingly, most of these cell types are derived from DE. We analyzed CCM pathways in the MH, and we found up-regulation of Covalent Chromatin Modification, Cell-Cell adhesion, Focal Adhesion, Cell Migration, Regulation of Actin Cytoskeleton, and Cell Proliferation. This data regarding Cell-Cell adhesion supports that MHs are undergoing CCM[19] (**Fig. 1K, Sup. Table 3**). We analyzed metabolic pathways and found up-regulation of lipid metabolism, DNA metabolic processes, and RNA metabolic processes (**Fig. 1L)**, and biosynthesis of amino acids, nucleotides, cholesterol, steroid, and fatty acid metabolism (**Fig. 1O)**. We also analyzed down-regulated pathways (**Fig. 1M, 1N, 1P, Sup. Tables 3-5)**, which included a down-regulation of CCM pathways and of both TCA cycle and oxidative phosphorylation genes. We also examined up-regulated and down-regulated pathways in the GT, MH, HB, and HM populations (**Sup. Figs. 1P-U, Sup. Tables 4-5**). Compared to the MH population, the HM populations also exhibit up-regulated CCM genes, and signaling pathways, but down-regulated liver differentiation genes.

To further substantiate the findings with DAVID, we developed a ranking approach for analyzing individual pathways based upon both the adjusted FDR level (0.3), and frequency of up-regulation (or down-regulation) in the sixteen possible comparisons between MH and the other (DE, GT, HB, and HM) cell populations. We found a list of 35 signaling/cognate receptor pathways, divided to obtain a list of 17 upregulated signaling pathways and 18 upregulated intracellular mediators (**Fig. 1O, Sup. Table 6**). We performed similar analysis for metabolic signaling pathways (**Fig. 1P, Sup. Table 6)**. One-third of metabolic pathways identified were lipid metabolism (combining Fatty acid and Cholesterol metabolism), with increased glyoxylate and dicarboxylate, 2-oxyglutarate, and 2-oxocarboxylic acid process, metabolites linked with fatty acid metabolism, hypoxia signaling and chromatin modification, and cell proliferation, respectively [20-21]. We then validated this analysis by performing analysis with ENRICHR (**Table 7**). Taken together, our ranking approach identified numerous up-regulated signaling and metabolic pathways.

We wanted to further delineate the MH phenotype. We performed focused heat map analysis on signaling (Hippo signaling, TGF-ß, Wnt, Pluripotency), Branching Morphogenesis, Migration, Hypoxia, Metabolism (Oxidative Phosphorylation, TCA cycle), and Master Liver Transcription Factors, with examples shown (**Fig. 1Q-R, Sup. Fig. 1V, Sup. Tables 6-7**). We observed a significant coordination of

gene expression in the MH population, with all pathways upregulated except Liver differentiation, Oxidative phosphorylation, and TCA cycle genes (**Fig. 1S, Table 7, Sup. Table 8)**, with mixed expression of Master Liver Transcription factors (**Sup. Table 9).** We hypothesized that FOXA1/2/3 may correlate with the coordinated changes in pathways, due to their role in liver differentiation and metabolism [22]. Interestingly, down-regulation of FOXA2 correlated with coordinated pathway changes (**Fig. 1T)**, suggesting FOXA2 expression may play a role We also validated our main findings of the MH population by analyzing a second scRNA-seq study of liver development (**Sup. Fig. 2A-H**) [18].

Design of a novel transplant model that supports the role for LD-MESC in early LO

Since changes in the E9.5 MH population were triggered in the E9.0 LD-MESC, we first modeled the hLD-MESC with an *in vivo* system. Murine LD-MESC growth is characterized by hypoxic growth, morphogenesis/CCM within MES tissues, and rapid ALB transcription. To model this, we employed hPSC-derived DE, which presumably would form HE *in vivo* [23] and human foreskin fibroblasts (HFF) to model the MESC. We employed two controls, hPSC alone, and a hepatoblastoma-derived (HepG2) cell line, in addition to the hPSC-DE (**Sup. Fig. 3C-E**) mixed with HFF. We transplanted tissues subcutaneously to preserve hypoxic conditions (**Fig. 2A**). All three conditions generated tissues in *vivo* after 4 weeks (**Fig. 2B**). hPSC alone formed teratoma-like tissues, as hematoxylin and eosin (H + E) staining highlighted the germ layers (**Figure 2C, left, middle, right panels)**. The hPSC-DE mixed with HFF and transplanted demonstrated that DE-derived cells formed cords of cells (blue) within the fibroblast mass (orange), indicative of hepatic cord morphogenesis, but with no apparent blood vessels (**Fig. 2D, left and middle panel**, **right panel (**highlighted by image segmentation**))**. Transplanted human HepG2 liver cells resulted in a homogeneous liver tissue architecture (**Fig. 2E, left and right panels)**. qRT-PCR showed that the DE:HFF condition had comparable AFP expression to the hepatoma control (**Fig. 2F, left panel)**, and the same levels of ALB as the teratoma control (**Fig. 2F, right panel)**. Therefore, the DE:HFF condition expressed high levels of ALB, and these values (~ 10^6) defined the upper limit of ALB transcription, demonstrating maturity. Importantly, both the teratoma and the DE:HFF condition were mixed samples that contained RNA of other contaminating cell types, and that likely the hepatic-specific RNA values were indeed higher. We determined the *in vivo* growth rate by estimating cell size initially and after 4 weeks, and compared to *in vivo* growth for 4 weeks [10] we observed a 40-fold increase in volume compared to *in vivo* eLO. Nonetheless, the data suggests that the hLD-MESC model exhibits hypoxic exponential growth, morphogenesis and CCM within MES tissue, and rapid ALB transcription, events that occur in the murine LD-MESC (**Fig. 2F, right panel)**.

Design of a novel and reproducible protocol for hPSC-HB induction with continuous mesenchymal signaling

Based upon our analysis of eLO and existing hepatic protocols (**Sup. File, Methods: Design of culture system**), we developed a novel hepatic induction protocol that involves continuous hypoxia, an absence of maturation factors, a reliance on spontaneous HB formation, and a single medium formulation. After hPSC-DE induction (**Sup. Fig. 3C-E**), we compared control, the GF (+) condition, based upon a published protocol [6], with the hepatic and mesenchymal (H + M) condition (1.1% KO serum), and a serum-free formulation (SFD), the GF (-) condition (**Fig. 2G**). The overall protocol (**Fig. 2H-I**) was applied to multiple embryonic stem cells (hESC) and hiPSC cell lines were tested with similar results. Day 4 hPSC-DE demonstrated cuboidal cells with bright cell borders (**Fig. 2J, top, left**). In the control, GF (+), condition, we observed a more elongated morphology by day 12 (**Fig. 2J, top, right**), whereas we observed more cuboidal epithelial morphology in the GF (-) and H + M conditions (**Fig. 2J, bottom left, bottom right**). In the H + M condition, we also observed both epithelial (E) and non-epithelial (NE) elements.

We first examined the effects of medium on gene expression. Although we did observe elevated levels of AFP and ALB (**Fig. 2K**), PROX1 was significantly upregulated in the H + M compared to GF (-) condition, which is normally expressed in both hepatic and extrahepatic biliary duct progenitors. Further, CDX2 was significantly downregulated in the H + M compared to GF (-) condition, and is expressed in hindgut and intestine (**Figure 2K**). Based on this data, as well as our time course data (**Fig. 2L**), we employed H + M in further experiments. ELISA analysis demonstrated a steady increase in ALB secretion from day 4 to 14, although ALB secretion was low compared to human functional HEPs in a stable culture system [24] (**Fig. 2M**). Next, we performed immunoanalysis of the GF (-) and H + M conditions (**Fig. 2N-Q, Sup. Fig. 3F-J**). We observed high AFP expression and low/intermediate levels of ALB expression for both conditions (**Fig. 2N**). In the day 6 H + M condition, we observed no ALB expression, low levels of CDX2 expression (mid and hindgut), and SOX2 (foregut), consistent with ventral foregut endoderm (**Fig. 2O**). In the day 14 H + M condition, we observed heterogeneous CD31 expression, but not in the GF (-) condition (**Fig. 2P**), consistent with transient endothelial expression in hepatogenesis [25]. Consistent with the early HB phenotype, we observed nuclear expression of FOXA2 and HNF4A in both the GF (-) and H + M conditions (**Fig. 2Q**). CDX2 expression was lower in the H + M condition compared to the GF (-) condition. Based on this, we term the H + M treated cells as an early hPSC-HB population. We performed long term culture in H + M medium, which showed an AFP, ALB, and TBX3 + cell population. This indicates that day 14 HBs were stable in hypoxic culture up to day 24 and presumably beyond (**Sup. Fig. 3K**).

Effects of medium on growth and CCM from hPSC-HB organoids in extracellular matrix droplets

Our next goal was to form compact organoids with the early hPSC-HBs, to recreate the hLD-MESC and trigger CCM, growth, and further early HB maturation. We performed experiments to elucidate factors which cause organoid compaction, or condensation. We found both H + M medium, and MES-derived cells, promote compaction (**Sup. Fig. 4A-G**). Similarly, for hPSC-HBs in H + M medium (modified EGM formulation) compaction resulted (**Fig. 3A-B)**, establishing that H + M favors organoid compaction. Immunostaining of organoids demonstrated evidence of both ALB expression (**Fig. 3C),** as well as other liver proteins (**Sup. Fig. 4F**) and hPSC-HB organoids were viable (**Sup. Fig. 4G**). Tissue sectioning demonstrated well-organized compact tissue with clusters of epithelial cells and several cystic regions (**Fig. 3D**). We then employed early hPSC-HB organoids to model the LD-MESC by transferring them to MG droplets under hypoxic conditions (**Fig. 3E, top**). 96-well systems submerged with MG showed similar results (**Fig. 3E, bottom**). When day 15, H+ M treated hPSC-HB organoids were transferred to MG droplets, control medium demonstrated minimal or no CCM by day 18 (**Fig. 3F, top two panels, inset)**, whereas H + M medium resulted in radial finger-like migrating protrusions with evidence of branching and webbing (**Fig. 3F, bottom two panels, inset)**, shown at higher magnification (**Fig. 3G**). We observed peripheral cystic structures in control medium-treated organoids (**Fig. 3G, left)**, and in the H + M condition, migrating, branching cell strands that extend well over 100 µm (**Fig. 3G, right)**. Filtering improved visualization of this phenotype (**Fig. 3H)**. Similar migrating strands were also observed in a 96-well plate model (**Fig. 3I**). Since it was challenging to observe and analyze 3D CCM, we analyzed adherent organoids, which were plated slightly lower in the MG droplet. In adherent organoids, we again observed minimal CCM in the control, but extensive CCM in the H + M treated condition (**Fig. 3J)**. The data indicates that CCM and growth were linked, as we observed significantly more growth area (outgrowths), and measures of CCM, in H + M treated adherent organoids compared to control organoids (**Fig. 3K**). We also evaluated collagen gels droplets instead of MG, which known to be stiffer (2 mg/ml) (**Fig. 3L**), and observed sheet-like growth in the H + M condition (**Fig. 3L, bottom panels and inset**) compared to control, which exhibited minimal growth (**Fig. 3L, top panels and inset**), with significant differences (**Fig. 3M, left**). Overall growth was significantly higher in H + M treated, MG organoids, compared to H + M treated, CG organoids (**Fig. 3M, right**). In summary, our data demonstrates that H + M medium stimulates growth and morphogenesis compared to control, and that MG induces collective branching, whereas CG induces sheet-like CCM. Moreover, our extracellular matrix droplet model models key aspects of the LD-MESC.

Day 18 LD-MESC organoids from extracellular matrix droplets express an immature hepatic signature in the absence of maturating factors

We hypothesized that the hLD-MESC model links migration with further maturation, in the absence of additional instructive/maturating factors. Gene expression analysis demonstrated that H + M medium resulted in significantly higher ALB, PROX1, and significantly lower TTR and TBX3 expression (**Sup. Fig. 5A)**. In the H + M condition, we determined how culture configuration (monolayer (MONO), compared to suspension (SUSP), and MG (MG and CCM) effects gene expression (**Fig. 4A**). Hepatic gene expression, in all cases, was significantly higher in both SUSP and MG compared to MONO. Cardiovascular gene expression was significantly higher for CD31 and NK2.5 in MONO compared to both SUSP and MG, but significantly lower for VEGFR2 for MONO compared to both SUSP and MG. Mesenchyme markers FOXF1 and RUNX2 were significantly lower in MONO compared to both SUSP and MG conditions. The gut markers SOX2, CK19, and PDX1 were unchanged between MONO and both SUSP and MG conditions, while CDX2 and EPCAM were both significantly upregulated in MONO compared to SUSP and MG conditions. Thus, in MONO culture, there is an increase in cardiovascular and gut gene expression, and decreased hepatic expression, as compared to SUSP and MG. When comparing SUSP and MG conditions, hepatic, cardiovascular and mesenchyme, and gut were equivalent except for TBX3, which was significantly higher in MG condition. Overall, the data suggests that compaction in H + M medium enhances differentiation, and that the MG condition, which exhibits CCM, maintains hepatic differentiation markers and upregulates TBX3 expression. Further, there are extensive increases in hepatic gene expression in SUSP and MG conditions compared to the MONO condition.

hLD-MESC model demonstrates liver protein expression and function

We hypothesized that the hLD-MESC model, which exhibits CCM, also co-expresses liver and mesodermal protein expression. This was based upon extensive mesoderm emergence from the LD [17], as well as the potential presence of HM cells [17]. Organoid immunostaining showed AFP was expressed in both the control and the H + M condition (**Fig. 4B top and middle panel**). We noted that the bright center will saturate the image with traditional thresholding and the intensity of the image had to be increased to visualize migrating strands at the edge. Using this approach, we found migrating strands were indeed AFP positive (**Fig. 4B, middle panel**), CD31 low (**Fig. 4C top, bottom panel**), TBX3 low (**Fig. 4D top, bottom panel**), and SMA high (**Fig. 4E, top, bottom panel**). We performed ELISA for ALB secretion (**Fig. 4F**). MONO condition showed low ALB secretion, ALB secretion was higher in SUSP vs. MG condition and the MG and SUSP condition were significantly lower than HepG2 cell secretion (**Fig. 4F)**. We then analyzed urea secretion. Urea secretion in MONO culture showed an

increase but then a significant decrease from ay 14-day 18. (**Fig. 4G)**. The MG condition secreted significantly more urea than the SUSP culture and NHDF condition and was significantly lower than HepG2 (**Fig. 4G)**. Thus, the MG condition demonstrated lower ALB secretion, but higher urea secretion when compared to the SUSP condition. We performed long term culture of day 18 hPSC-HBs in MG droplets until day 30 (**Fig. 4H**). Morphological analysis shows progressive rapid and irregular growth accompanied by CCM (**Fig. 4H**). Immunoanalysis demonstrates stable ALB expression (**Fig. 4H**, **middle and bottom rows**). This suggests the cells are stable and robust in long culture. Overall, our data suggests that the migrating hPSC-HBs display an AFP +, ALB +, and SMA + population, suggesting a partial mesenchymal phenotype, and secreted higher urea than SUSP organoids, and demonstrating robust culture through at least Day 30.

Early hPSC-HBs exhibit a functional mesenchymal phenotype in a functional assay with bioengineered tissue culture platform

Numerous studies demonstrate a hepato-mesenchymal (HM) hybrid phenotype arises during early development [17,26], and mouse fetal liver [27] and these cells could provide leader cells for CCM [19] and potentially provide a niche for hematopoietic stem cells in the fetal liver [26]. We wanted to test the hypothesis of whether day 18 H + M treated cells exhibited a functional, mesenchymal, HM phenotype. We used an established bioengineered device that evaluates tissue tension in mesenchymal-derived microtissues [28]. The device is a microfabricated pillar culture system predicated upon supporting formation of a microtissue with mesenchymal properties. We performed a series of preliminary experiments with cell lines to establish the requirement of mesenchyme for forming a hepatic microtissue and measuring tissue tension (**Sup Figs. 6A-F**). Day 18 hPSC-HBs robustly formed microtissue in the microfabricated pillar culture system, indicating a mesenchymal phenotype (**Fig. 4I-J**). We performed contractile tension analysis, and demonstrated the hPSC-HB microtissue generated tension, but at significantly lower levels than the HUVEC and HUVEC-HepG2 systems (**Fig. 4K**). Thus, these data support the premise that day 18 HBs bear a HM phenotype.

Screening of pathway inhibitors demonstrates that Hippo pathway controls triggering of LO

Our bioinformatic analysis demonstrated that E9.5 MH is associated with an up-regulation of numerous signaling pathways, which are immediately downregulated (E10.5) (**Fig. 1K, 1O, 1U**). We identified 35 potential candidate signaling pathways in eLO, and here we tested pathway activity in the day 18 hLD-MESC adherent organoid model by performing an *in vitro* chemical screen with 3 criteria (**Methods and Fig. 5A**). After the addition of chemical inhibitors (control, Y27632, LDN, SB41352, VT)

at the highest doses, we observed significant reduction in growth/CCM in response to the VT treatment (**Fig. 5B**). We then expanded our screen to twenty-four inhibitor conditions (based on **Fig. 1U**), with eight candidates (three concentrations per candidate). We performed dose responses up to three orders of magnitude (**Sup. Table 10**). We identified inhibition of CCM/growth for A83-01 (high), Cristozinib (high), LDN (high), SB43152 (high), SU5416 (intermediate dose), Verteporfin (VT) (high, intermediate), but not for Wortmannin, or Y27632 (**Fig. 5C, red arrows**). Interestingly, at intermediate doses, the only inhibitors that significantly reduced CCM were VT and SU5416. We hypothesized that the lack of CCM/growth at the highest concentrations could be due loss of cell viability, rather than just blocking CCM/growth. Indeed, we found that all inhibitors except SU5416 and Y27632, caused cell death at highest doses, and were removed (**Fig. 5D-E**). The two remaining inhibition conditions at intermediate doses were SU5416 and VT, which we found decreased CCM/growth but did not increase cell death (**Fig. 5F**), and thus were positive hits of the screen. Given the success of VT in our screen, and our global analysis of scRNA-seq data demonstrating Hippo pathway activation (**Fig. 1R**), we concluded Hippo pathway (YAP-TEAD signaling) plays a key role in linking growth and CCM. To support this, we re-analyzed murine scRNA-seq data for mediators of Hippo, and we found that they were all upregulated in the MH population (**Fig. 5G**). Next, analysis of gene expression of Hippo mediators in the day 18 hLD-MESC system showed that in the MG condition, YAP1 and MST1 was significantly upregulated in the MG condition compared to control, MST2 was significantly downregulated to control, with no differences in TAZ, LATS1, TEAD2, TEAD4 (**Fig. 5H**). In summary, our chemical screen recovered VT as a positive hit. Analysis of Hippo mediators in the MH population and in the hLD-MSC model suggest growth/CCM is linked to changes in Hippo pathway.

DISCUSSION

LO is a central, cross disciplinary topic in regenerative medicine, and hPSC are a valuable tool for interrogating LO, bringing together basic and practical applications. Progress in the field of LO has been comprised of significant genetic studies, and both single cell RNA-seq analysis and hPSC-HEP studies, but

eLO has yet to be scrutinized. In fact, current hPSC approaches do not account for eLO. Based on the premise that the E8.5-10.5 stage LD-MESC is significant for linking signaling with CCM, growth, and differentiation, we employed bioinformatics analysis, and both *in vivo* hPSC and *in vitro* hPSC investigation, to not only elucidate the transcriptome of the E9.5 MH cells, but also to develop more accurate models of these developmental stages. We have obtained several novel findings that push forward the field of LO, including novel 3-step protocol and medium formulation, a new cell population

that has not previously has been induced or isolated, a simple but effective *in vivo* model, extensive knowledge and analysis of the E9.5 niche and transcriptome, and a molecular mechanism involved in hPSC liver organoid growth/CCM. In terms of accuracy of modeling the LO, our simple *in vivo* model transplant model demonstrates exponential growth at approximately the rate of *in vivo* liver growth [10] and our *in vitro* model demonstrates rapid ALB activation, collective cell migration, and growth, function of immature HBs, and establishment of the hepatic nuclear GRN (FOXA1, FOXA2, FOXA3, HNF1α, HNF1ß, HNF4α, HNF6, HEX, TBX3, and PROX1) [15]. Our 3-step culture platform be used as an initial step in hPSC-HEP differentiation, and our study will serve as a resource for the LD-MESC. The clinical implications of our work are for understanding and treating migrating or metastasizing hepatocellular carcinoma and for evaluating the therapeutic role for both LD-MESC concept and MHs in human liver repopulation.

Our bioinformatics analysis of the eLO process provides a full resource of the LD-MESC and how it triggers eLO via MH cells, which opens up many potential areas of investigation. Based upon our data here, we extend our description of the events of eLO to comprise not only increased signaling, CCM, exponential growth, and rapid differentiation, but also metabolic programming, emergence of MES-derivatives, and the role for nascent liver immune system in growth. These integrated transformations that arise provide numerous research directions for future investigation in this crucial area. While functional analysis is still required, our data indicates that the MH cells, arising from the LD-MESC, have a unique transcriptomic signature, with elevated signaling, immune pathways, and stress responses. Interestingly, we found upregulated signaling pathways in MH are also predominantly upregulated during murine liver regeneration. Overlapping pathways between MHs and regenerating hepatocytes include C-met (HGF receptor), EGFR, FGFR, Wnt, TGF-ß, VEGFR, Hippo, Notch, IGF-1, NIK/NF-kB, p21, p53, TNF, IL-6, and endocannabinoids [29-30]. Moreover, the upregulated list of signaling pathways in MH is the surprising balance in number between traditional soluble signaling pathways and immune signaling pathways. Our REACTOME (pie chart) analysis demonstrated an increase in up-regulation in immune system signaling, and the ENRICHR pathways confirmed the list of potential immune signaling pathways, including TNF, IFN-γ, Oncostatin, Interleukins (IL-1, IL-2, IL-4, IL-5, IL-6, IL-11, IL-12, IL-18) as well as B and T cell-receptor signaling, NIK/NF-kB, and Calcineurin-NFAT signaling. Finally, the upregulated pathways include an extreme pattern of the global cell stress response, a pattern that included HIF1α (oxygen), AMPK (energy), mTOR (nutrient), FoxO (oxidative), DNA damage-related stress, with evidence of endoplasmic reticulum (ER) stress. Additionally, we observed the activation of PI3K-Akt, suggesting PI3-AKT-mTOR axis is active in the MH cells, which is active also in cancers [31]. This unique transcriptome suggests that the eLO deserves further attention in hPSC protocols and can be used to model cancer.

Notably, in the E9.5 MH population, not only was Hippo signaling clearly upregulated in the E9.5 MH population, it was identified independently in our novel hPSC protocol and chemical screen for mechanisms of CCM and growth. Hippo pathway integrates mechanical forces (integrins and Rho signaling), intercellular adhesion, WNT signaling, and stresses (osmotic, oxygen, energy) to alter YAP/TAZ signaling, leading to CCM and growth [32]. Consistent with Hippo signaling and increased CCM, lung branching morphogenesis genes were also upregulated, which has not previously been reported (**Fig. 1S**). Further, our in-depth analysis of Hippo mediators with heatmaps in the 9.5 MH population, and in the hLD-MESC, as well as the results of our chemical screen for signaling pathways in hLD-MSC, all pointed towards a major role for Hippo (YAP-Tead) [33] in not only mediating migration, but also linking migration with growth and differentiation. Our data collectively implicates Hippo in integrating not only signaling pathways with migration/growth/differentiation, but also metabolic programming, stress pathways, biomechanical niche, and chromatin modification/epigenetics. Further studies with our model can be employed to discover potential mechanisms by which this integration may occur.

There are several limitations to our study worth mentioning. Regarding our choice of medium, we employed a modified derivative of EGM-2 medium which is a commercially available and has a proprietary medium formulation, and does not reveal the basal medium composition nor does it reveal the concentrations of Heparin, EGF, R3-IGF (Repligen), FGF, or VEGF. Nonetheless in the future, multifactorial experiments need to be performed to determine which factors, at which doses, result in maximal ALB activation. Another limitation is that although we present robust, long-term culture of the day 14 early HB or the day 18 migrating HBs, and we presented evidence of hepatic-specific functions in both cases, we have not fully differentiated the cells. This would involve simply applying maturating factors, which are established in the field. In summary, our hLD-MESC model is unique culture system which links migration, growth, and differentiation, can be used for *in vivo* tissue growth, and exhibits signaling pathways not seen in monolayer culture. This novel LD-MESC model can serve as a platform further investigation into early LO. Further, enhanced imaging analysis of organoids, with techniques like spatial transcriptomics [34] and knockout and functional studies of VEGFR and EGFR, will help determine mechanisms of CCM and the phenotype of the leader cells.

METHODS

Bioinformatics Analysis

We performed scRNA-seq analysis of published eLO data. Further details in **Sup. Files (Sup. Methods)**.

In vivo transplantation assay

We modeled the hLD-MESC *in vivo*. Further details in **Sup. Files (Sup. Methods)**.

Design of culture system

We modeled the hLD-MESC *in vivo*. Further details in **Sup. Files (Sup. Methods)**.

All other methods in the **Sup. Files (Sup. Methods)**.

Note-The techniques for in vitro differentiation and in vivo transplantation are protected by a provisional patent

Acknowledgements:
NP was supported by the UB CBE startup funds, a Mark Diamond Fellowship, the New York State Stem Cell Science C024316, the UB the Stem cells in regenerative medicine (ScIRM) center, the University at Buffalo Center for Cell, Gene, Tissue Engineering (CGTE). OO was supported by the Western NY Prosperity Fellowship. We would like to thank Drs. Jeremy Lotto and Pamela Hoodless (University of British Columbia), for assistance regarding the bioinformatics figure. We would like to thank Dr. Imtiaz Mohammed (Lead histologist) and Dr. Amber Worral (PAS Microscopy and Histology Core Labs Director) for their assistance with tissue preparation, processing and sectioning of our tissue samples within the histology core facility at the University at Buffalo. We would also like to thank Dr. Wade Sigurdson (Confocal Microscope and Flow Cytometry Facility Director) for his advice on methods of imaging tissues and whole-mount organoids.

AUTHOR CONTRIBUTIONS:

OO, DG, ST, AC, TN, DB, CO, AK, CS, PC, SR, ZC, PJ, SM, RZ, RG, NP: Supervising the work, Responsible for all data, figures, and text, Ensuring the authorship is granted appropriately, Ensuring that the authors approve the content and submission of the paper, Ensuring that all authors approve the content and submission of the paper, as well as edits made through the revision and production processes, Ensuring adherence to all editorial and submission policies, Identifying and declaring competing interests on behalf of all authors , Identifying and disclosing related work by any co-authors under consideration elsewhere, Archiving unprocessed data and ensuring that figures accurately present the original data.
NP: Arbitrating decisions and disputes and ensuring communication with the journal (before and after publication), sharing of any relevant information or updates to co-authors, and accountability for fulfillment of requests for reagents and resources.

Declaration of Interests:

NP is founder of Livandala, a pre-seed stage biotech company that develops stem cell treatment for chronic liver disease. The other authors hereby state no competing interest involved with the ideation, writing, or revision of this manuscript.

FIGURES

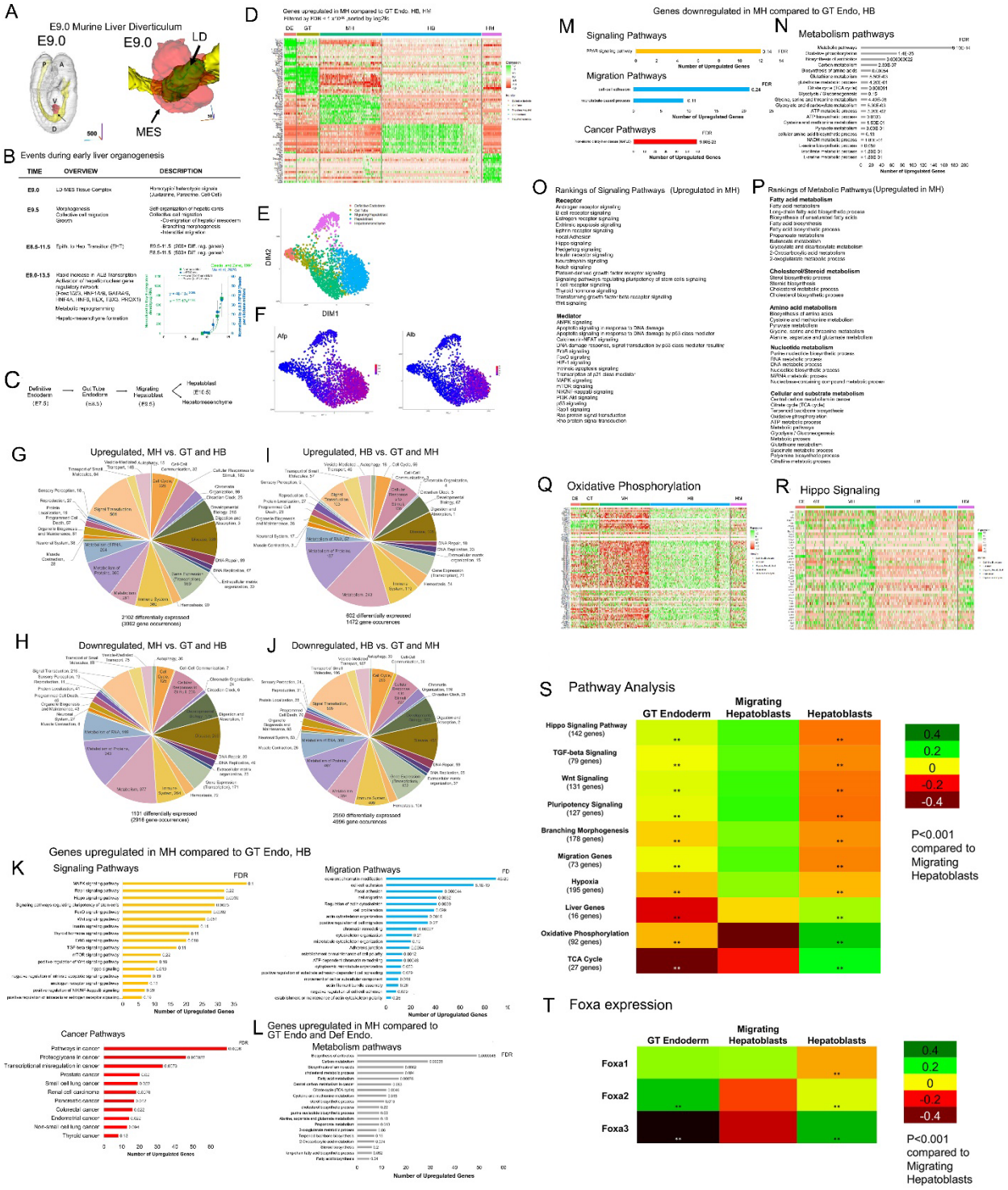

Figure 1. Bioinformatics analysis of murine scRNA-seq data during early LO demonstrates coordinated transcriptomic changes during CCM

A) 3D images of the E9.0 Liver Diverticulum (LD) (right) (adopted from [10]). LD (green) is shown to be surrounded by mesodermal-derivatives (MES) (red).

B) Description of early murine LO between E8.5-13.5. Double plot shows correlation from our analysis scRNA-seq [17] and Northern blot [16] .

C) Hepatic lineage map used in this study.

D) Heatmap filtered for FDR < 1×10^{-20} and sorted by log2-fold-change.

E) A force-directed layout plot (n = 2332 cells), from clustered based on re-grouping.

F) Force-directed layout plot analysis of liver differentiation markers (Alpha-fetoprotein (AFP), Albumin (ALB)).

G-J) Pie chart created with REACTOME containing gene categories for DEG lists (log2fc > 0.5,FDR < 0.05). Total DEG and the number of gene occurrences shown.

K-L) Upregulated pathways (GO BP, Kegg, DAVID) for MH vs. GT and HB. For metabolic pathways, for MH vs. DE and GT was used.

M-N) Same as above except downregulated (log2fc < -0.5, FDR < 0.05) gene list.

O-P) Ranked, alphabetically sorted, upregulated pathways (GO BP, Kegg) for both signaling (O) and metabolism (P).

Q-R) KEGG oxidative phosphorylation pathway (Q) and GO BP hippo signaling pathway (R) Heatmaps

S) Pathway heatmap analysis, with averaged value, for select pathways for GT, MH, and HB cells ** is p < 0.001.

T) Heatmap for FOXA factors. Analysis same as in S).

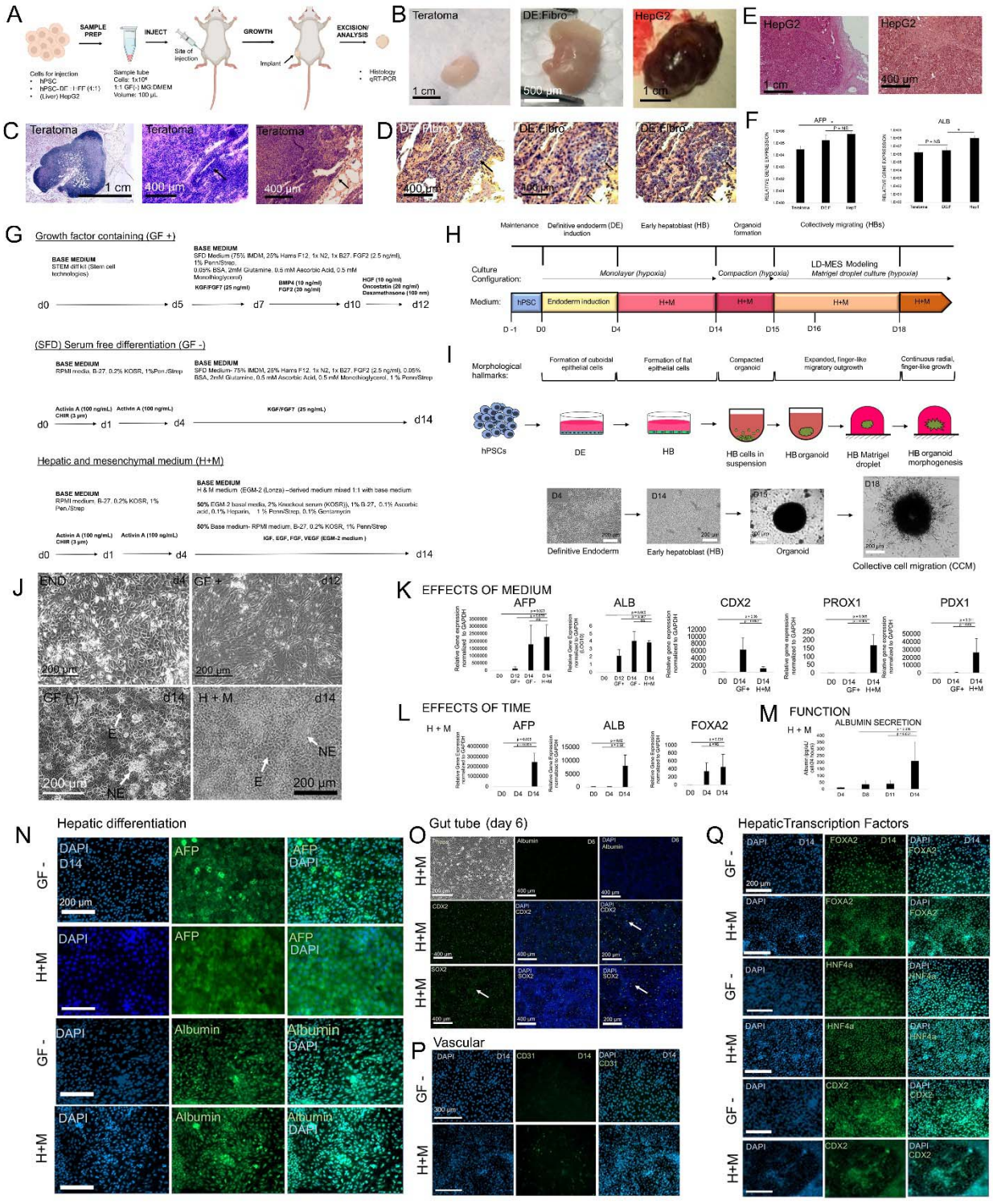

Figure 2. ***In vivo*** **transplantation protocol and** ***in vitro*** **protocol for modeling early LO.**

A) Schematic of 4-week, hLD-MESC transplant (NOD-SCID) model, with hPSC-DE:HFF (4:1 ratio) plus GF-free MG subcutaneously transplanted.

B) Gross images of teratoma, hPSC-DE:HFF, HEPG2 tumor, 4 weeks post-transplantation.

C-E) Histological analysis (Hematoxylin and Eosin) of Teratoma (neuro-tubular structures (arrow), connective tissue (arrow)); hPSC-DE:HFF (DE-derived (blue) (arow), HFF (orange)), last image segmented; HEPG2 tumor

F) Bar graph of qRT-PCR gene expression *in vivo* human liver differentiation. AFP/ALB (n = 3), DE:F (n = 5), HEPG2 (n = 4), mean ± SD.

G) Three protocols for hPSC-HB induction (5% O_2); Growth factor (GF (+)) protocol based upon published work [55]; GF (-) protocol with serum-free SFD medium, H + M protocol EGM-2 modified medium.

H) Overall schematic summarizing 3 stages for the H + M differentiation protocol. Early hepatoblast (HB) stage-day 4-14 in monolayer; Compaction stage – day 14-15; LD-MESC stage- organoid in MG droplet.

I) Same as H, except morphological hallmarks are shown.

J) Morphological analysis during HB differentiation. Endoderm (END)-cuboidal; GF (+): elongated; GF (-) : cuboidal; epithelial (E) and non-epithelial (NE) elements (arrows); H + M condition: cuboidal, and NE elements.

K) Gene expression analysis (qRT-PCR) of the effects of medium on hepatic differentiation; GF (+) (n = 3), GF (-) (n =3), and H + M (n = 4); mean ± SD.

L) Same as K except effects of time: day 0 (n = 3), day 4 (n = 3), and day 14 (n = 3); mean ± SD.

M) Enzyme-linked immunoabsorbance assay (ELISA) analysis for ALB secretion; day 8 (n = 4), day 11 (n = 5), day 14 (n = 3). mean ± SD.

N) Immunocytochemistry of day 14 hPSC-derived HBs in H + M and GF (-) conditions. DAPI (UV filter), FITC, and merged (UV and FITC) are shown. HBs are stained for AFP (above) and ALB (below).

O) Same methods as in H) except hPSC-derived GT endoderm (day 6 cells) were stained by immunocytochemistry, and ALB (liver), CDX2 (hindgut), and SOX2 (foregut) were targeted.

P) Same methods as in H) except CD31 (vascular differentiation) was targeted.

Q) Same methods as in H) except hepatic TFs FOXA2, HN4A, and gut TFs were assessed targeted, as was the intestinal marker CDX2.

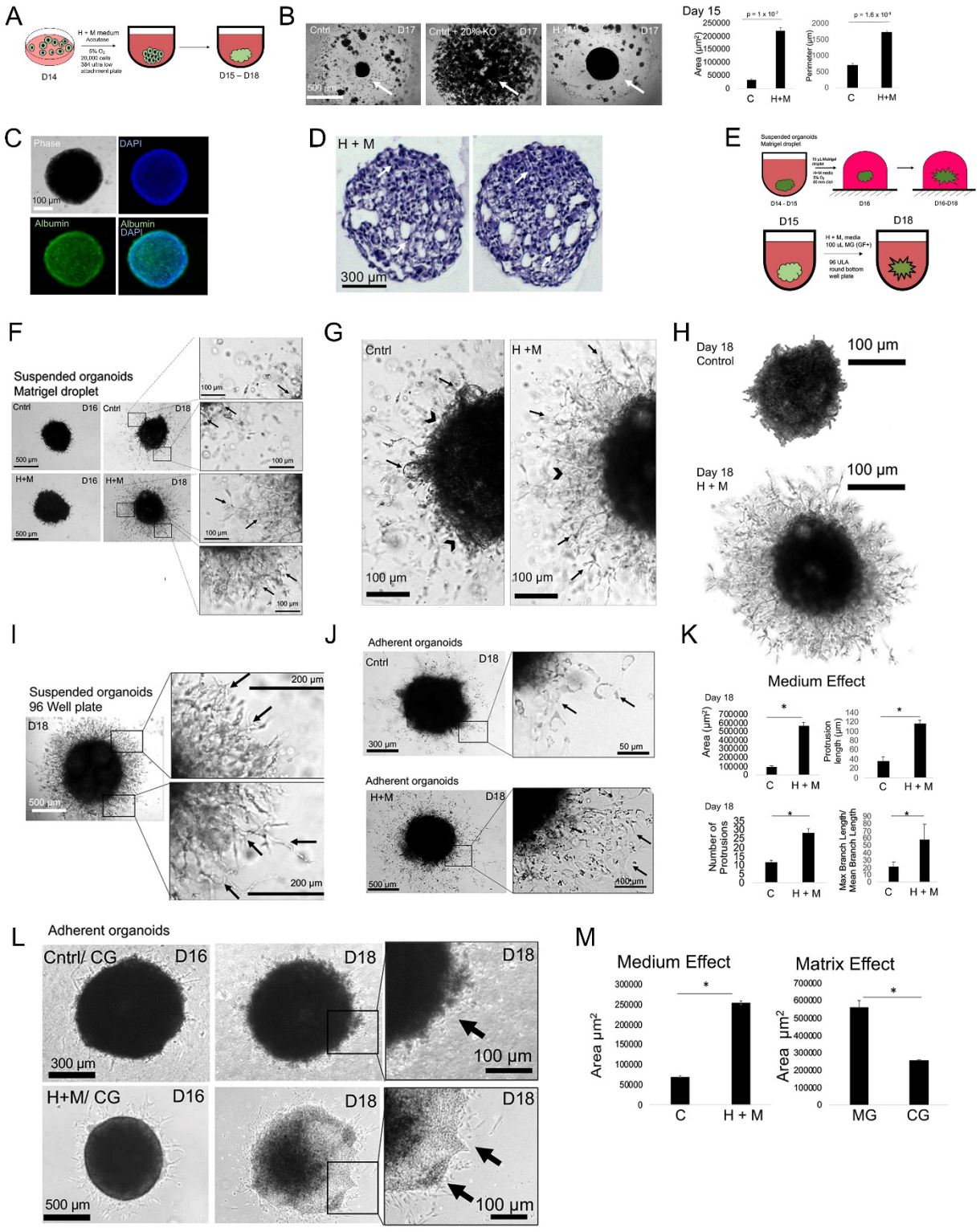

Figure 3. Induction of CCM from hPSC-derived HB organoids

A) Schematic of day 14 hPSC-HB organoid formation

B) Day 17 images hPSC-HB organoid compaction. Left: control RPMI basal; Middle: RPMI basal medium + 20% KOSR; Right: H + M; Right: Bar graph quantitation: Area (n = 4), perimeter (n = 4); mean ± SD.

C) Immunofluorescence staining of ALB (middle row), on day 17 hPSC-HB whole organoids.

D) H + E images of day 17 hPSC-HB organoids; above arrows- uniform epithelium; below arrows- non-uniform- cystic like structure.

E) Schematic of day hPSC-HB organoid suspended in Matrigel (MG) droplet culture (60 mm dish) or 96-well.

F) Phase contrast images of day 18 migrating hPSC-HBs treated in control and H + M medium.

G) Same as F except larger; Control: cyst like structures (arrow), minimal CCM (arrowhead). H + M organoids (right) demonstrate CCM.

H) Same as F except filtered images to remove out cells that were out of focus.

I) Phase contrast images of H + M treated hPSC-HB organoids, on day 18 in 96-well plate format. Extensive radial CCM is demonstrated.

J) Phase contrast images of control (arrow: minimal CCM) and H + M treated (arrow: CCM) hPSC-HB an adherent organoid model.

K) Bar graphs analysis of images in I-J. Area ($P = 3 \times 10^{-4}$), protrusion length ($P = 2.8 \times 10^{-4}$), number of protrusions ($P = 1.4 \times 10^{-3}$), and the max /mean branch length ratio ($P = 1.4 \times 10^{-2}$), mean ± SD.

L) Same as J except collagen gel (CG); c images of control (arrow: minimal CCM) and H + M treated (arrow: CCM)

M) Bar graphs analysis in adherent CG droplets. Left: Effects of medium for CG; Right- Effects of MG vs CG for H + M treated.

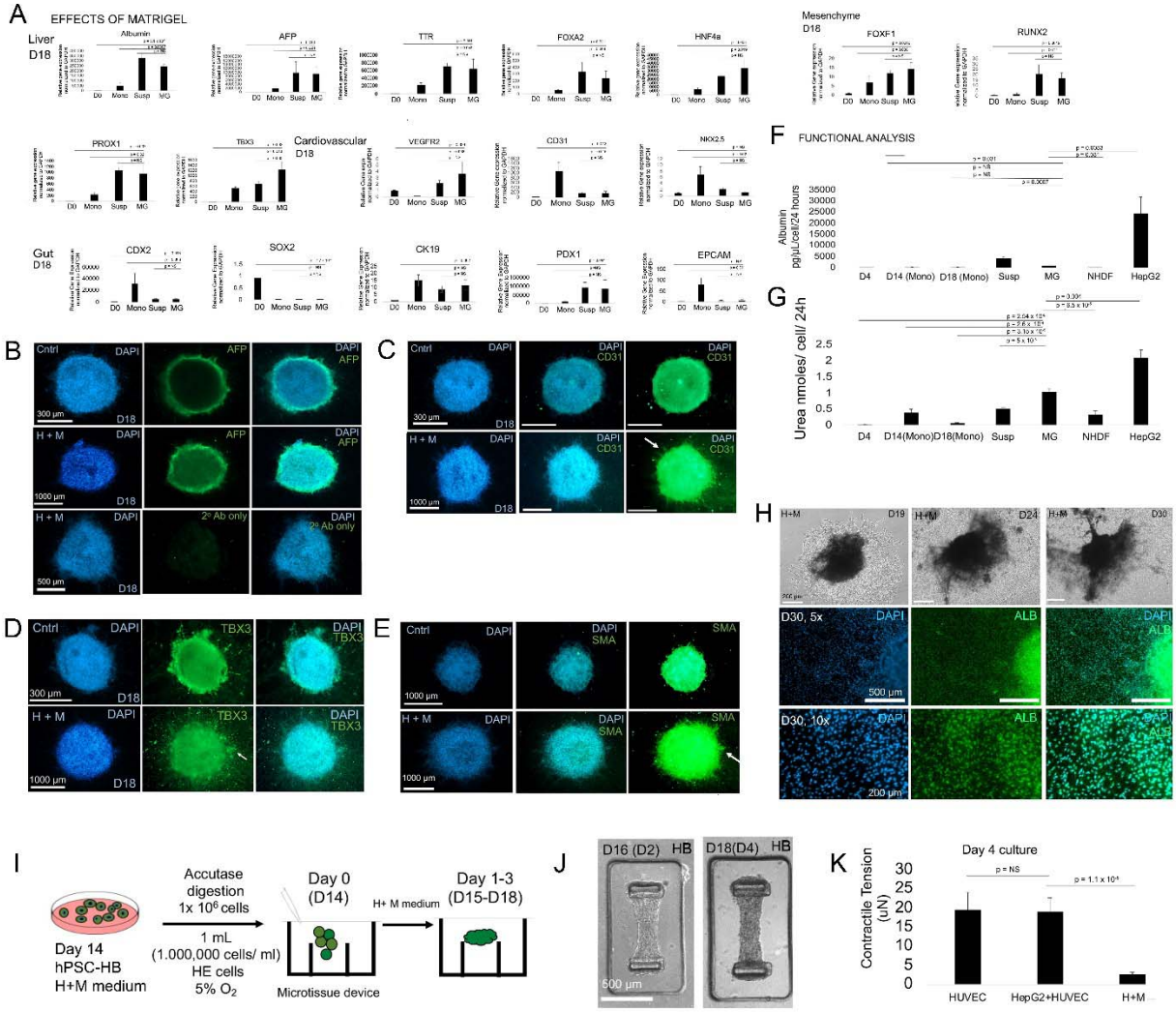

Figure 4. Gene and protein expression of control and H + M organoids cultured in MG droplets.

A) Gene expression analysis comparing day 18 monolayer (Mono), day 18 suspended organoids (Susp), and day 18 MG droplet (MG) conditions in H + M medium conditions. Day 0 (n = 3), Mono (n = 3), Susp (n = 3), and MG (n = 3). p-values shown; mean ± SD.

B-E) Immunocytochemistry of Control (top) and H + M treated (Middle and lower) day 18 whole organoids for AFP (B), CD31 (C), TBX3 (D), SMA (E); counterstained with DAPI and FITC.

F) ELISA analysis ALB secretion of day 4 (n = 3), day 14 MONO) (n = 3), day 18 MONO (n = 3), day 18 (SUSP), day 18 organoids (n =3), NHDF cells (n = 3), HepG2 liver hepatoblastoma (n = 3); p-values listed; mean ± SD.

G) Same as F, except urea secretion analysis. Conditions measured were same as in I. p-values listed; mean ± SD.

K) Long term MG droplet culture organoids; Top: day 19, 24, 30 images; Middle: ALB Immunofluorescence; Lower-Same as previous except at higher magnification.

L) Schematic demonstrating culture of hPSC-HB in microdevices; day 14 hPSC-HB are harvested and replated in device in H + M medium.

M) Phase contrast image of microtissues in microdevices that form on day 2 (day 16, left) and thicken by day 4 (day 18, right).

N) Graph of contractile tension in microtissue; hPSC-HB (n = 6), HUVEC/HepG2 (n = 3); p-values shown; mean ± SD.

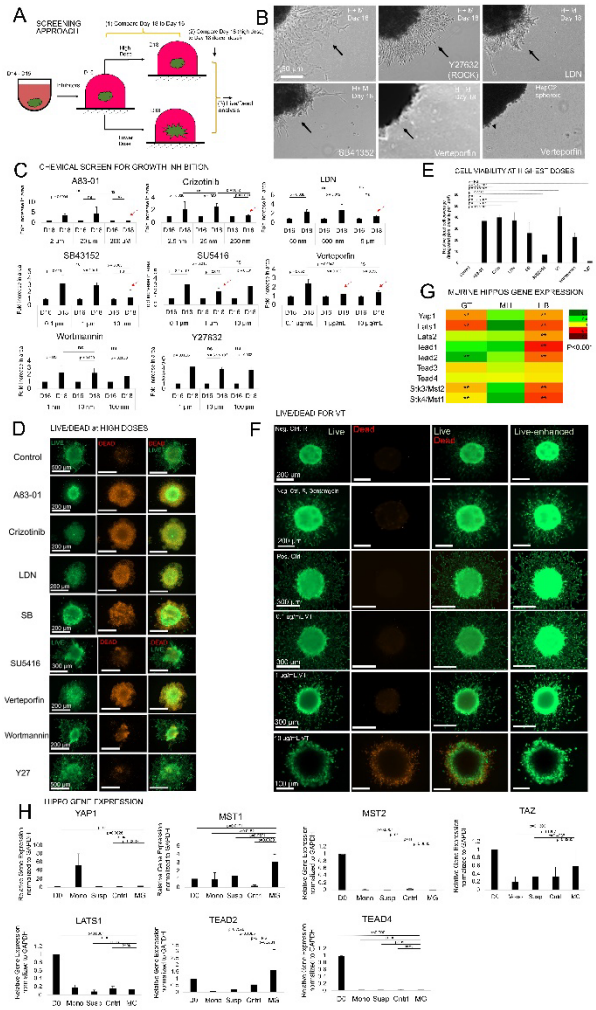

Figure 5. Functional screen of small molecule signaling pathway inhibitors for inhibition of CCM in hPSC-HB organoids in MG droplet culture.

A) Schematic of functional chemical screen of signaling pathways that effect organoid growth/migration.

B) Images of treated organoids. Top- untreated control, ROCK treated, LDN treated; Bottom- SB41352 treated, Verteporfin (VT) treated, and HepG2 spheroids + V treated; Arrows show inhibition.

C) Data for each inhibitor screened; Fold-increase in area (growth) with 3 concentrations per chemical inhibitor; Red arrows indicate positive hits; P-values listed; n = 3 for each condition. Plotted is mean ± SD.

D) Images of live (green) /dead (red) assay for cell viability after chemical treatment.

E) Quantitation of experiments in D); P-values shown; N =3 per condition; mean ± SD.

F) Same as D but focused on VT treatment; enhanced images (green) shown.

G) Heatmap analysis of averaged hippo pathway mediator gene expression from mouse scRNA-seq data (Lotto et al.) ** $p < 0.01$.

H) Hippo gene expression analysis in day 18 organoids; Monolayer (MONO), Suspension (SUSP), Control (CNTRL), MG (Migrating). One-way ANOVA using Tukey's multiple comparison test; mean ± SD.

REFERENCES

1 Marcellin, P. & Kutala, B. K. Liver diseases: A major, neglected global public health problem requiring urgent actions and large-scale screening. *Liver Int* **38 Suppl 1**, 2-6, doi:10.1111/liv.13682 (2018).

2 Ogoke, O., Oluwole, J. & Parashurama, N. Bioengineering considerations in liver regenerative medicine. *J Biol Eng* **11**, 46, doi:10.1186/s13036-017-0081-4 (2017).

3 Zaret, K. S. Regulatory phases of early liver development: paradigms of organogenesis. *Nat Rev Genet* **3**, 499-512, doi:10.1038/nrg837 (2002).

4 Si-Tayeb, K., Lemaigre, F. P. & Duncan, S. A. Organogenesis and development of the liver. *Dev Cell* **18**, 175-189, doi:10.1016/j.devcel.2010.01.011 (2010).

5 Si-Tayeb, K. *et al.* Highly efficient generation of human hepatocyte-like cells from induced pluripotent stem cells. *Hepatology* **51**, 297-305, doi:10.1002/hep.23354 (2010).

6 Takebe, T. *et al.* Vascularized and functional human liver from an iPSC-derived organ bud transplant. *Nature* **499**, 481-484, doi:10.1038/nature12271 (2013).

7 Shinozawa, T. *et al.* High-Fidelity Drug-Induced Liver Injury Screen Using Human Pluripotent Stem Cell-Derived Organoids. *Gastroenterology*, doi:10.1053/j.gastro.2020.10.002 (2020).

8 Koike, H. *et al.* Nutritional modulation of mouse and human liver bud growth through a branched-chain amino acid metabolism. *Development* **144**, 1018-1024, doi:10.1242/dev.143032 (2017).

9 Velazquez, J. J. *et al.* Gene Regulatory Network Analysis and Engineering Directs Development and Vascularization of Multilineage Human Liver Organoids. *Cell Syst* **12**, 41-55 e11, doi:10.1016/j.cels.2020.11.002 (2021).

10 Ogoke, O. *et al.* Spatiotemporal imaging and analysis of mouse and human liver bud morphogenesis. *Dev Dyn* **251**, 662-686, doi:10.1002/dvdy.429 (2022).

11 Sugiyama, Y. *et al.* Sinusoid development and morphogenesis may be stimulated by VEGF-Flk-1 signaling during fetal mouse liver development. *Dev Dyn* **239**, 386-397, doi:10.1002/dvdy.22162 (2010).

12 Rossi, J. M., Dunn, N. R., Hogan, B. L. & Zaret, K. S. Distinct mesodermal signals, including BMPs from the septum transversum mesenchyme, are required in combination for hepatogenesis from the endoderm. *Genes & development* **15**, 1998-2009, doi:10.1101/gad.904601 (2001).

13 Hentsch, B. *et al.* Hlx homeo box gene is essential for an inductive tissue interaction that drives expansion of embryonic liver and gut. *Genes & development* **10**, 70-79, doi:10.1101/gad.10.1.70 (1996).

14 Sosa-Pineda, B., Wigle, J. T. & Oliver, G. Hepatocyte migration during liver development requires Prox1. *Nat Genet* **25**, 254-255, doi:10.1038/76996 (2000).

15 Lau, H. H., Ng, N. H. J., Loo, L. S. W., *et. al*. The molecular functions of hepatocyte nuclear factors - In and beyond the liver. *J Hepatol* **68**, 1033-1048, doi:10.1016/j.jhep.2017.11.026 (2018).

16 Cascio, S. & Zaret, K. S. Hepatocyte differentiation initiates during endodermal-mesenchymal interactions prior to liver formation. *Development* **113**, 217-225 (1991).

17 Lotto, J. *et al.* Single-Cell Transcriptomics Reveals Early Emergence of Liver Parenchymal and Non-parenchymal Cell Lineages. *Cell* **183**, 702-716 e714, doi:10.1016/j.cell.2020.09.012 (2020).

18 Mu, T. *et al.* Embryonic liver developmental trajectory revealed by single-cell RNA sequencing in the Foxa2(eGFP) mouse. *Commun Biol* **3**, 642, doi:10.1038/s42003-020-01364-8 (2020).

19 Friedl, P. & Gilmour, D. Collective cell migration in morphogenesis, regeneration and cancer. *Nat Rev Mol Cell Biol* **10**, 445-457, doi:10.1038/nrm2720 (2009).

20 Kunze, M., Pracharoenwattana, I., Smith, S. M. et al. A central role for the peroxisomal membrane in glyoxylate cycle function. *Biochim Biophys Acta* **1763**, 1441-1452, doi:10.1016/j.bbamcr.2006.09.009 (2006).

21 Herr, C. Q. & Hausinger, R. P. Amazing Diversity in Biochemical Roles of Fe(II)/2-Oxoglutarate Oxygenases. *Trends Biochem Sci* **43**, 517-532, doi:10.1016/j.tibs.2018.04.002 (2018).

22 Friedman, J. R. & Kaestner, K. H. The Foxa family of transcription factors in development and metabolism. *Cell Mol Life Sci* **63**, 2317-2328, doi:10.1007/s00018-006-6095-6 (2006).

23 Wang, A. *et al.* Epigenetic priming of enhancers predicts developmental competence of hESC-derived endodermal lineage intermediates. *Cell Stem Cell* **16**, 386-399, doi:10.1016/j.stem.2015.02.013 (2015).

24 Bader, A. *et al.* A stable long-term hepatocyte culture system for studies of physiologic processes: cytokine stimulation of the acute phase response in rat and human hepatocytes. *Biotechnol Prog* **8**, 219-225, doi:10.1021/bp00015a007 (1992).

25 Goldman, O. *et al.* KDR identifies a conserved human and murine hepatic progenitor and instructs early liver development. *Cell Stem Cell* **12**, 748-760, doi:10.1016/j.stem.2013.04.026 (2013).

26 Chagraoui, J., Lepage-Noll, A., Anjo, A., *et al*. Fetal liver stroma consists of cells in epithelial-to-mesenchymal transition. *Blood* **101**, 2973-2982, doi:10.1182/blood-2002-05-1341 (2003).

27 Li, B., Zheng, Y. W., Sano, Y., *et al*. Evidence for mesenchymal-epithelial transition associated with mouse hepatic stem cell differentiation. *PLoS One* **6**, e17092, doi:10.1371/journal.pone.0017092 (2011).

28 Xu, Y., Koya, R., Ask, K. , *et al*. Engineered microenvironment for the study of myofibroblast mechanobiology. *Wound Repair Regen* **29**, 588-596, doi:10.1111/wrr.12955 (2021).

29 Tao, Y., Wang, M., Chen, E. , *et al*. Liver Regeneration: Analysis of the Main Relevant Signaling Molecules. *Mediators Inflamm* **2017**, 4256352, doi:10.1155/2017/4256352 (2017).

30 Bohm, F., Kohler, U. A., Speicher, T. , *et al*. Regulation of liver regeneration by growth factors and cytokines. *EMBO Mol Med* **2**, 294-305, doi:10.1002/emmm.201000085 (2010).

31 Yap, T. A. *et al.* Targeting the PI3K-AKT-mTOR pathway: progress, pitfalls, and promises. *Curr Opin Pharmacol* **8**, 393-412, doi:10.1016/j.coph.2008.08.004 (2008).

32 Moya, I. M. & Halder, G. Hippo-YAP/TAZ signalling in organ regeneration and regenerative medicine. *Nat Rev Mol Cell Biol* **20**, 211-226, doi:10.1038/s41580-018-0086-y (2019).

33 Alder, O. *et al.* Hippo signaling influences HNF4A and FOXA2 enhancer switching during hepatocyte differentiation. *Cell reports* **9**, 261-271, doi:10.1016/j.celrep.2014.08.046 (2014).

34 van den Brink, S. C. *et al.* Single-cell and spatial transcriptomics reveal somitogenesis in gastruloids. *Nature* **582**, 405-409, doi:10.1038/s41586-020-2024-3 (2020).